RESEARCH ARTICLE

WILEY **Journal of RAMAN SPECTROSCOPY**

Bone quality assessment of osteogenic cell cultures by Raman microscopy

Gurjit S. Mandair[1] 🆔 | Pieter Steenhuis[1] | Michael A. Ignelzi Jr[2] | Michael D. Morris[3]

[1] Department of Biologic and Materials Sciences, School of Dentistry, University of Michigan, Ann Arbor, Michigan

[2] Department of Orthodontics and Pediatric Dentistry, School of Dentistry, The University of North Carolina, Chapel Hill, North Carolina

[3] Department of Chemistry, University of Michigan, Ann Arbor, Michigan

Correspondence
Gurjit S. Mandair, Department of Biologic and Materials Sciences, School of Dentistry, University of Michigan, Ann Arbor, MI.
Email: gmandair@umich.edu

Funding information
NIH, Grant/Award Numbers: DE11530, P30 AR069620 and R01 AR047969

Abstract

The use of autologous stem/progenitor cells represents a promising approach to the repair of craniofacial bone defects. The calvarium is recognized as a viable source of stem/progenitor cells that can be transplanted in vitro to form bone. However, it is unclear if bone formed in cell culture is similar in quality to that found in native bone. In this study, the quality of bone mineral formed in osteogenic cell cultures were compared against calvarial bone from postnatal mice. Given the spectroscopic resemblance that exists between cell and collagen spectra, the feasibility of extracting information on cell activity and bone matrix quality were also examined. Stem/progenitor cells isolated from fetal mouse calvaria were cultured onto fused-quartz slides under osteogenic differentiation conditions for 28 days. At specific time intervals, slides were removed and analyzed by Raman microscopy and mineral staining techniques. We show that bone formed in culture at Day 28 resembled calvarial bone from 1-day-old postnatal mice with comparable mineralization, mineral crystallinity, and collagen crosslinks ratios. In contrast, bone formed at Day 28 contained a lower degree of ordered collagen fibrils compared with 1-day-old postnatal bone. Taken together, bone formed in osteogenic cell culture exhibited progressive matrix maturation and mineralization but could not fully replicate the high degree of collagen fibril order found in native bone.

KEYWORDS
bone quality, osteogenic differentiation, Raman microscopy, stem cells, tissue engineering

1 | INTRODUCTION

Bone defects, particularly of the craniofacial complex, are a complication of trauma, congenital malformation, or tumor surgery.[1–3] Despite significant advances in craniofacial bone repair, there is an additional risk of bone loss through postoperative bone resorption, infection, abnormal bone healing, or radiotherapy.[3–6] Small bone defects and bone losses can be repaired using autologous bone grafts, but for more extensive repairs and repeated surgeries, alloplastic bone substitutes or banked bone allografts can be used.[6,7] Other promising biomaterials for craniofacial bone repair include tissue-engineered constructs,[8] which are ideally seeded with osteogenic stem/progenitor cells sourced from the patient's own body.[9–11] Although the use of autologous stem/progenitor cells would overcome issues of immunorejection, challenges still remain in identifying

suitable human bone-forming cells that meet the clinical need, including the need to assess the quality of bone formed in preclinical models.[7,11–13]

Stem/progenitor cell selection and enrichment are two of several important prerequisites that need to be satisfied in developing tissue-engineered therapies for craniofacial bone repair.[14] In mice, the stem cell antigen (Sca-1) is widely used to enrich hematopoietic stem cells, including stem, progenitor, and differentiated cells from a variety of tissue types, such as bone marrow, bone, muscle, cardiac, vascular endothelium, and skin.[15] By combining cell sorting with negative Sca-1 selection, enriched stem and/or progenitor cell fractions can be obtained from neonatal or adult mice. Recent studies have shown that fetal and postnatal mouse calvaria can also provide a source of osteogenic stem/progenitor cells, which can be enriched by negative Sca-1 immunomagnetic selection (Sca-1$^-$).[16,17] Sca-1$^-$ cell fractions can form bone in vitro or be loaded into absorbable gelatin sponges and then transplanted into mice to form bone in vivo.[17]

Sca-1 expression is known to vary between different mouse strains and tissue types,[12,18] and thus it would be necessary to evaluate their osteogenic potential and the quality of bone formed in vitro. Evaluation of osteogenic potential becomes apparent considering that Sca-1$^-$ and positive Sca-1 (Sca-1$^+$) cell selection can also be used to enrich chondroprogenitor and adipoprogentior cells, respectively, and thus, if given the appropriate culture conditions, would form their corresponding cartilage and adipose tissue types.[16,17] Current osteogenic assays include alkaline phosphatase (ALP) to detect osteoblastic differentiation and histochemical mineral stains, such as von Kossa and Alizarin Red, to quantify phosphate and calcium levels in vitro, respectively. However, mineral stains are nonspecific,[19,20] and thus cell culture studies would also benefit from complementary bone quality assessments performed by Raman or Fourier-transform infrared spectroscopy (FTIR).

Raman spectroscopy can be used to follow the osteogenic differentiation of various cell phenotypes in culture,[21] as well as document the real-time formation and accumulation of bone mineral in cell or organ culture systems.[22,23] In this static time-dependent study, Raman microscopy and mineral stains were used to examine the bone-forming potential of Sca-1$^-$ stem/progenitor cells derived from fetal mouse calvarias. The relative quantity and maturity of the bone mineral formed over a 28-day culture period was also compared against reference measurements obtained from postnatal calvarial tissues. Given the high plating densities of cells used in this study and their spectroscopic resemblance to type I collagen, the feasibility of using Raman microscopy to assess cell activity and bone matrix quality were also examined.

2 | MATERIALS AND METHODS

2.1 | Sca-1$^-$ cell isolation, plating, and osteogenic differentiation

All experiments were approved by the Institutional Animal Care and Use Committee (UCUCA) at the University of Michigan.[16] Calvarial tissues of 18.5 fetal-day-old B6CBAF1/J mice were harvested and cells obtained by sequential enzymatic digestion.[16] Sca-1$^-$ cell fractions were plated, expanded, and incubated using standard cell cultivation techniques.[16] Confluent Sca-1$^-$ cells were passaged once prior to replating at 10,000 cells/cm^2 on sterilized fused-quartz slides (S1-UV grade, 12.7-mm circulars, Esco Products, Oak Ridge, NJ). Fused-quartz slides were used because of their low Raman background compared with glass[24,25] and their ability to maintain cell proliferation and morphology.[26,27] At confluence, expansion media was replaced by osteogenic culture media (Dulbecco's Modified Eagle Medium-low glucose containing 2% fetal bovine calf serum, 10 mM β-glycerophosphate, 0.1 μM dexamethasone, and 0.2 mM ascorbic acid 2-phosphate) to induce osteogenic differentiation.[16,28] The osteogenic media was refreshed every 2–3 days.

2.2 | Raman microscopy and spectral acquisition.

At the following time intervals: 1, 4, 8, 14, 17, 25, and 28 days ($n = 3$ slides per time interval), the osteogenic culture media was removed, and quartz slides were rinsed once with phosphate-buffered saline solution and fixed with ice-cold 70% ethanol.[29] After air-drying the slides in a laminar flow hood, they were sampled using Raman microscope equipped with a 785 nm laser.[25] The spectrograph was fitted with a 50-μm slit to provide a spectral resolution of 6–8 cm^{-1}. The excitation laser was spot-focused through a 50 × 0.80 numerical aperture (NA) objective (Nikon Instruments, Inc.,) to give ~23 mW laser power at the sample. The slide was placed onto a gridded reference slide (Electron Microscopy Sciences, Hatfield, PA) to allow the sampled sites to be relocated and reimaged after von Kossa staining. For each sample slide, 12–18 spectra were acquired from suspected mineralizing sites. Spectra were acquired using 12-min acquisition times. All sample and calibration spectra were processed in MATLAB® software (The MathWorks Inc., Natick, MA) using locally written scripts.[25]

2.3 | Mineral staining

After spectral analysis, one set of sample slides were stained for inorganic phosphate using the von Kossa technique described elsewhere.[17] The remaining slides were stained for calcium using a freshly prepared and filtered 1% Alizarin Red solution (pH ~4.2).[29] After 2 min, the dye solution was removed and the slides rinsed with deionized water to remove any nonspecific binding of the dye to the extracellular matrix (ECM). Mineral formed by Sca-1⁻ cells cultured in a single 15-mm-diameter polystyrene well plate at Day 28 was also prepared and stained for calcium.[16] All Alizarin Red-stained cell quartz slides and polystyrene well plate were imaged using a SMZ800 stereomicroscope (Nikon Instruments, Inc.,).

2.4 | Spectroscopic reference materials

Fresh cortical calvarial tissues were harvested from postnatal Day 1 (PN1)- and postnatal Day 56 (PN56)-old male B6CBAF1/J mice ($n = 3$ per group).[16,25] Parietal-suture-parietal calvarial tissue sections were isolated, cleaned, and stored in a petri dish containing calcium-buffered saline solution at 4°C. Prior to Raman spectroscopic sampling, the tissue section was placed flat onto a quartz slide. For each tissue section, six spectra were acquired from the mineralized cortical parietal regions on either side of the central suture region using the acquisition parameters outlined above. Raman spectra were also acquired from the following reference materials: bovine Achilles type I collagen (Sigma Aldrich Co., St Louis, MO); triglyceride mixtures (Sigma Aldrich Co.,); synthetic powdered hydroxyapatite (HA; $n = 3$, Catalogue # 289396 with lot numbers: MKBC4763, MKBK2210V, and 06616CS; Sigma Aldrich Co.,); Gly-Pro-Hyp synthetic peptide (Bachem Biosciences Inc., King of Prussia, PA); and calf joint proteoglycan (Elastin Products Co., Inc. Owensville, MO). All materials were used as received, except for the triglycerides in which 4 μL aliquots on a fused-quartz slide were allowed to air-dry prior to acquisition.

2.5 | Curve-fit spectral analysis

Sample spectra were imported into GRAMS/AI® software (ThermoGalactic Inc., Salem, NH) for further processing. Briefly, background spectra of bare fused-quartz and sample slides were normalized to the intensity of the silica band at ~786 cm⁻¹, followed by spectral subtraction and smoothing using the Savitisky-Golay function (second-order polynomial, 7-point of smoothing).[24,30] Manual baseline correction was then applied to the 740–1,750 cm⁻¹ spectral region, followed by normalization to the intensity of the amide I C=O band at ~1,666 cm⁻¹. Spectra showing evidence for bone mineral (around $v_1(PO_4^{3-})$ band between 955 and 960 cm⁻¹) were separated from spectra containing mainly bone matrix (around resolvable v(C—C) protein backbone band at ~939 cm⁻¹). Spectra containing strong lipid δ(=CH) band at ~1,295 cm⁻¹ or glycosaminoglycan (GAG) δ (CH₃) band at ~1,378 cm⁻¹ were excluded because of their potential overlap with the major matrix proline v(C—C) and amide I v(C=O) bands at ~854 and ~1,666 cm⁻¹, respectively. The sharp band at ~1,554 cm⁻¹ in some spectra was identified as an optical artifact and thus can be ignored.

For curve-fit analysis, second-derivative and constrained Gaussian deconvolution functions were applied to the following spectral regions: 740–910, 900–990, 1,185–1,400, and 1,630–1,710 cm⁻¹. Tentative band assignments for the following key osteogenic culture components were made: cell tryptophan (Typ) protein band at ~757 cm⁻¹; cell nucleic acid v(P—O—P) band at ~782 cm⁻¹; matrix proline v(C—C) band at ~854 cm⁻¹; mineral $v_1(PO_4^{3-})$ band between 955 and 960 cm⁻¹; amide III v(C—N) + δ(N—H) bands at ~1,246 cm⁻¹ (α-helical or ordered structure) and ~1,264 cm⁻¹ (β-sheet or disordered structure); and amide I v(C=O) bands at ~1666 cm⁻¹ (nonreducible trivalent collagen crosslinks) and ~1,693 cm⁻¹ (reducible divalent collagen crosslinks).[31–33] Band position, bandwidth, and/or intensity ratios between select Raman bands, which contained information on cell activity and bone quality, were extracted.[31,34] Briefly, the mineral crystallinity parameter was calculated from the bandwidth of the mineral $v_1(PO_4^{3-})$ band at full width at half maximum.[31] Mineral/matrix ratios were derived from the mineral $v_1(PO_4^{3-})$ and proline v(C—C) band intensities.[27,31,35] Nucleic acid/Typ, collagen disorder/order, and collagen crosslinks ratios were based on: 781/854, 1,246/1,264, and 1,666/1,693 cm⁻¹ ratiometric parameters, respectively.[31] Lipid/matrix ratios were not calculated because of the possible dissolution of lipids by ethanol during the fixation step.[34] In addition, given that all spectra were acquired using a high-NA objective, we advise that the intensity of the amide III subband at ~1,270 cm⁻¹ used to calculate the 1,240/1,270 cm⁻¹ ratios may also exhibit some polarization dependence.[36,37]

2.6 | Statistical analysis

Statistical analyses were performed in SPSS Statistics Software for Windows (IBM SPSS Statistics Version 24, IBM Corp., NY). All results are presented as means ± standard

derivations (*SD*s). Due to the small sample size of $n = 3$ per group, power analyses between Day 8, Day 28, PN1, PN56, and/or HA comparisons were performed in nQuery Advisor Software using the Satterhwaite *t*-test.[38] Only Raman spectroscopic results that were sufficiently powered to claim statistical significances at 80% power (two-sided, $\alpha = 0.05$) were reported in this study. Two-tailed independent sample *t*-tests with Bonferroni corrections were then applied to comparisons between Day 8, Day 28, PN1, PN56, and/or HA groups (34 simultaneous tests). Statistically significant differences were considered at the $p < 0.0015$ (0.05/34) level. Bar plots and the regression plot were created using the software, Microsoft Excel 2010. The linear correlation between mineral crystallinity and band position of the mineral $v_1(PO_4^{3-})$ vibration was examined and the R^2 value and equation of the line reported.

3 | RESULTS AND DISCUSSION

3.1 | Temporal mineralization of Sca-1⁻ cell cultures

Sca-1⁻ cells took 3–4 days to achieve confluency on fused-quartz slides and displayed normal spindle- to oval-shaped morphologies that were similar to those observed previously on polystyrene plates.[16,17] As shown in Figure S1a–g, mineral formed by osteogenic Sca-1⁻ cell cultures were visualized by Alizarin Red staining at various time intervals over the 28-day culture period. Mineral-like deposits were first detected at Day 8. Thereafter, the frequency, size, and complexity of the mineralized bone nodules increased with culture time. The heterogeneous distribution of the bone nodules was expected given that primary Sca-1⁻ cells were passaged only once prior to replating and thus retained their mixed osteogenic stem/progenitor cell phenotypes.[39] The appearance of the bone nodules formed on the quartz slide at Day 28 (Figure S1g) resembled those formed on polystyrene culture plate at Day 28 (Figure S1h) in this study and in a previous study using the von Kossa staining technique.[16]

3.2 | Spectroscopic components of osteogenic cell cultures

Prior to evaluating the quality of bone formed in culture, it was necessary to spectroscopically characterize the key cell culture components formed under osteogenic differentiation with assistance from mineral staining techniques. Figure 1 shows the von Kossa stain images taken at specific time intervals over the 28-day culture period with site-matched spectra. As shown in

Figure 1e, cultures were not stained black for inorganic phosphate until Day 8. The associated spectrum shown in Figure 1f contained the distinct mineral $v_1(PO_4^{3-})$ band at ~958 cm⁻¹,[31] which was absent from the adjacent nonmineralized ECM region. On the basis of our analyses using reference spectra obtained from type I collagen (Figure S2a) and synthetic collagen Gly-Pro-Hyp tripeptide (Figure S2b), spectra obtained between Days 1 and 4 were dominated by cell-specific trypto-phan, nucleic acid, and tyrosine bands at 757, 782, and 827 cm⁻¹, respectively.[32,34] No clear collagen-specific bands were found, at least not until significant mineral deposition had occurred. For this reason, the band at ~854 cm⁻¹ was assigned to the collagen proline v(C—C) vibration between Days 8 and 28, but at earlier time intervals this band would contain greater contributions from cell tyrosine δ(C—C—H), valine v(C—C), and/or polysaccharide γ(C—O—C) vibrations.[31,32] The extent of spectral mixing between cell and collagen would also depend on the height of the bone nodule from the ECM layer, including the number of cells present at the surfaces or embedded inside the bone nodules.[39–41] Spectral mixing effects may also apply to the amide III, CH₂-wag, and amide I regions between 1,200 and 1,320, 1,420 and 1,500, and 1,630 and 1,700 cm⁻¹, respectively.[31]

A major lipid cell culture component was also identified. As shown in Figure S3a,b, a spectrum taken from the poorly mineralized region at Day 17 contained bands at 890, 920, 1,061, 1,128, 1,177, 1,295, 1,441, 1,727, and 1,741 cm⁻¹. These bands were characteristic of triglycerides, and their band positions coincided with those shown in the reference spectrum of the triglyceride mixture in Figure S2c and those reported in the literature.[42] Although bone triglycerides have been detected by chromatography[43] and NMR spectroscopy,[44] this is the first study in which they have been detected under osteogenic differentiation conditions by Raman microscopy. Previous studies have shown that primary osteogenic Sca-1⁻ cells have some limited capacity to form lipid vacuoles after 21 days under adiopogenic differentiation conditions.[17] These findings support other studies, which have proposed that osteogenic cell lineages can also produce lipids.[45,46]

Spectra acquired from the more granular region at Day 14 (Figure S3c,d) also gave rise to additional set of bands that were distinct from cell proteins, bone mineral, and triglycerides. The bands at 854, 939, 1,045, 1,081, 1,125, 1,339, and 1,419 cm⁻¹ resembled type I collagen but were more pronounced, whereas the CH₂-wag band between 1,452 and 1,458 cm⁻¹ was broader and more symmetrical when compared with that typically encountered for type I collagen (Figure S2a). The band at
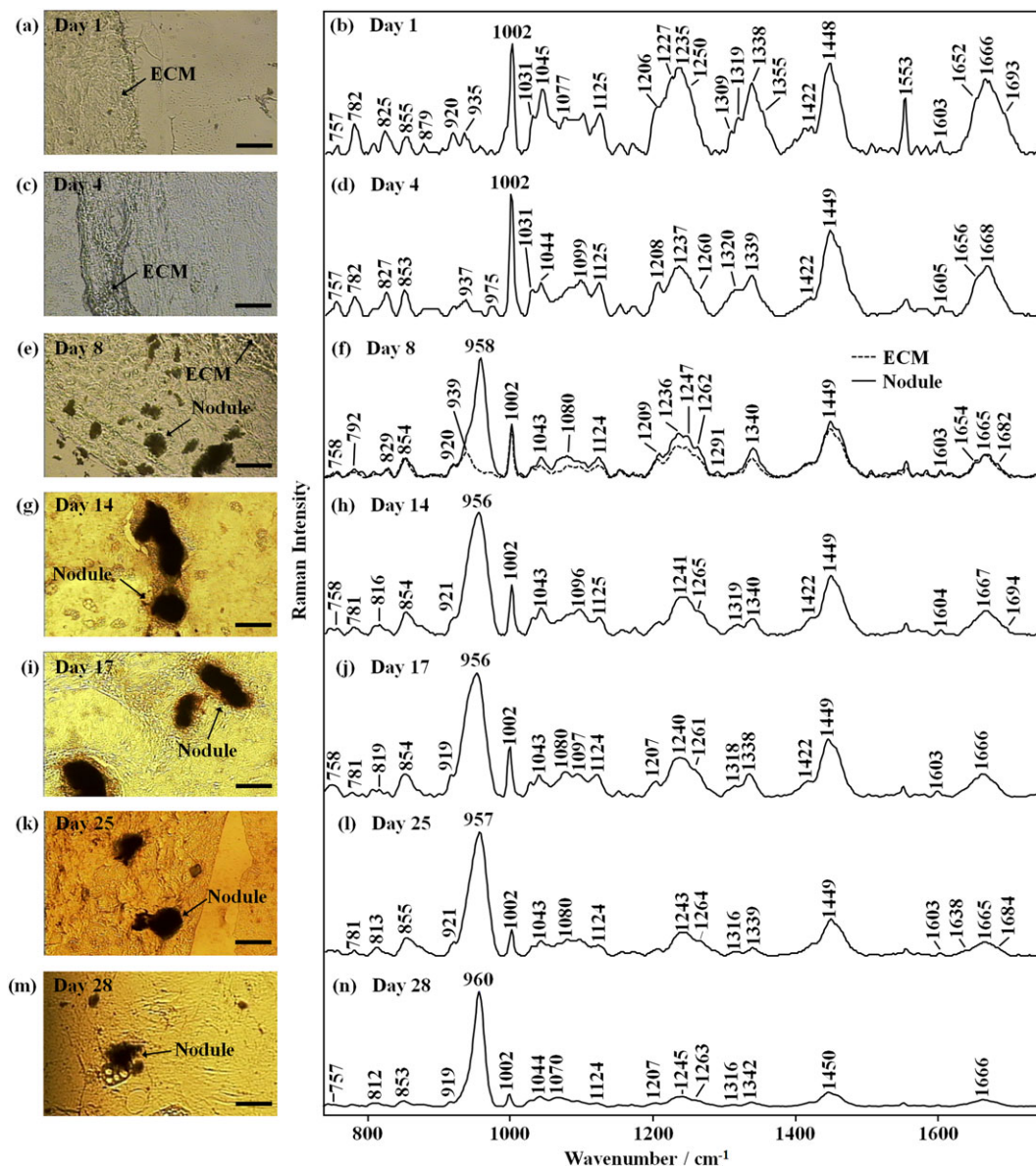
FIGURE 1 Select von Kossa-stained images with corresponding site-matched Raman spectra (see arrows) acquired at select cell culture days. (a, b) Day 1; (c, d) Day 4; (e, f) Day 8; (g, h) Day 14; (i, j) Day 17; (k, l) Day 25; and (m, n) Day 28. Scale bar: 200 μm [Colour figure can be viewed at wileyonlinelibrary.com]

~1,377 cm^{-1} in Figure S3e was also not typical of type I collagen. As shown in Figure S3d, the von Kossa image acquired from the granular region was not stained for inorganic phosphate and thus indicated the presence of a soluble ECM component. We propose that some of these additional bands, especially the band at 1,377 cm^{-1} originated from the δ (CH$_3$) bending mode of proteoglycans and/or glycosaminoglycans (GAGs), which have been reported to occur at ~1,375 cm^{-1} in subchondral bone.[33] The presence of proteoglycans and/or GAGs in our osteogenic cultures was also supported by the reference spectrum obtained from proteoglycan (Figure S3),

which also contained the δ (CH$_3$) band at ~1,374 cm^{-1}. More importantly, proteoglycans and GAGs are known to be expressed by calvarial tissues and preosteoblast cells, because of their importance in mediating cell proliferation and differentiation activities, as well as mineralization in an inhibitory and/or stimulatory manner.[47–50]

After key cell culture components had been characterized, curve-fit analyses were performed to extract information on cell activity and mineralization. The phase of the mineral formed in culture was also examined using the mineral crystallinity parameter and the mineral v_1(PO$_4$$^{3-}$) band position, whereas collagen crosslinks

and disorder/order ratios were used to evaluate the quality of the matrix. These spectroscopic parameters will be discussed in turn, including how bone formed at Day 28 compared with that of calvarial tissues obtained from postnatal mice at Day 1 (PN1) and Day 56 (PN56).

3.3 | Nucleic acid/protein ratios

Cell activities were evaluated using nucleic acid/protein ratios, which had previously been used to determine the differentiation and/or proliferation status of embryonic stem cells and primary mouse osteoblast cells.[27,51] Nucleic acid/protein ratios can be obtained from the ratio of the cell nucleic acid ν(O—P—O) band at ~782 cm^{-1} to

one of the cell protein tryptophan (Typ), proline (Pro), or general matrix CH_2-wag bands at 757, 853, or 1,450 cm^{-1}, respectively.[27,34,51] Given that Sca-1$^-$ cell cultures would eventually produce collagen and triglyceride components, nucleic acid/Typ ratio was considered as the most representative measure of early cell activity. As shown in Figure 2a, nucleic acid/Typ ratios declined dramatically after Day 1 because of the increased differentiation of Sca-1$^-$ osteoprogenitor/stem cells into the more mature osteoblast cell phenotype. The decline in nucleic acid/Typ ratios is most likely explained by increased matrix synthesis with differentiation, with DNA levels remaining constant as cell proliferation is downregulated.[52] Given that mineral deposition was first detected at Day 8, the downregulation in cell proliferation
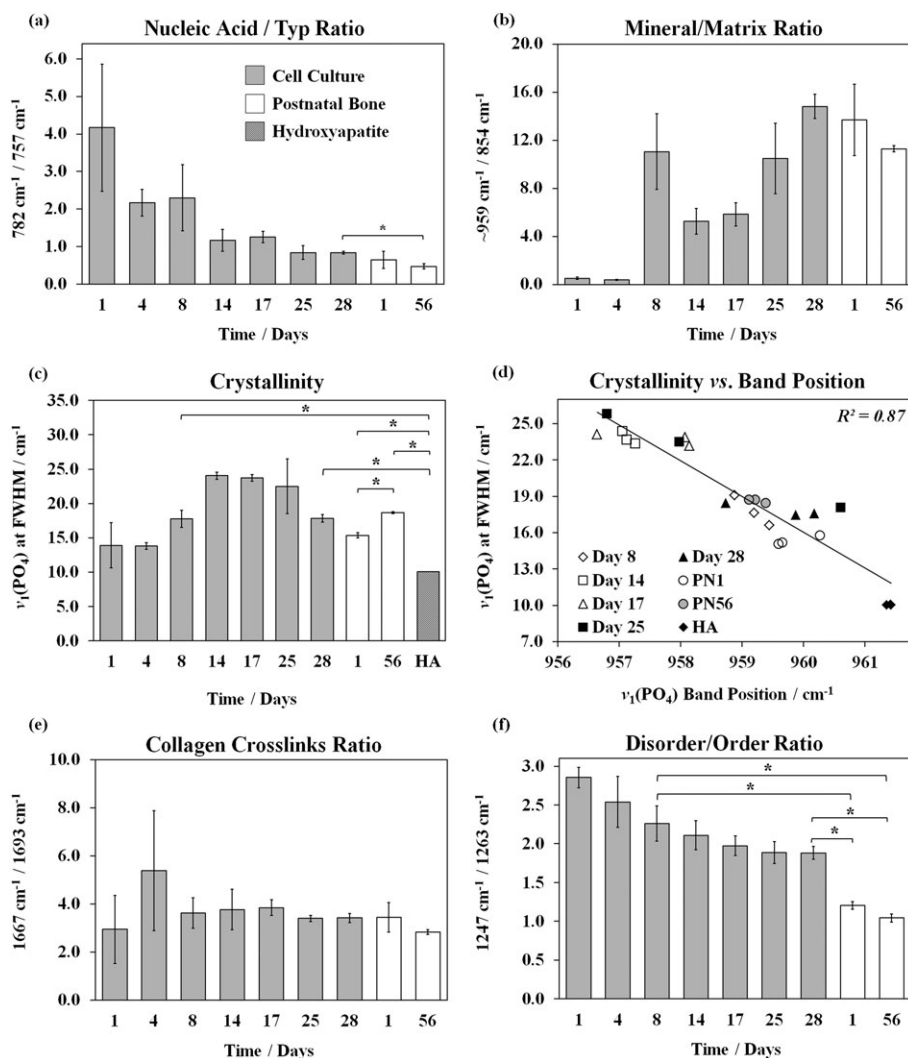

FIGURE 2 Raman spectroscopic bar plots obtained from osteogenic cell cultures (Days 1–28, shaded bars), postnatal bone (PN, 1 and 56 days old, white bars), and synthetic hydroxyapatite (HA, hatched bar in Figure 2c). Raman spectroscopic parameters detail the temporal changes in (a) cell activity, (b–d) bone mineral quality, and (e and f) bone matrix quality. Significant statistical differences between cell culture (8 or 28 days old), postnatal bone (1 and/or 56 days old), or synthetic HA groups were at the $p < 0.0015$ (*) level. (d) Shows the linear regression (R^2) correlation between mineral crystallinity and mineral $\nu1$(PO_4^{3-}) band position (y = −2.95x + 2848.4, $p < 0.001$)

would have occurred prior to this time point. Although nucleic acid/Typ ratios appeared to decline consistently throughout the 28-day culture period, we advise against using this parameter once significant mineralization has occurred because (a) the downregulation in cell proliferation is linked to increased matrix synthesis[52] and that (b) with increased incubation time, the cell-specific Typ protein band at 757 cm^{-1} would gain greater spectral contributions from collagen.

3.4 | Mineral/matrix ratios

The mineralization of osteogenic cultures was evaluated using mineral/matrix ratios derived from the mineral $v_1(PO_4^{3-})$ band between 955 and 960 cm^{-1} and the matrix proline band at 853 cm^{-1}. As shown in Figure 2b, mineral was not detected spectroscopically until Day 8, which was later confirmed by von Kossa staining (Figure 1e,f). However, mineralization decreased on Day 14 but then increased again between days 17 and 28. This bimodal mineralization behavior contrasts with the linear mineralization trends reported throughout the 28-day culture period for human primary osteoblast (HOb) and osteoblast-like U20S cells.[53] The bimodal mineralization trend found in this study could in part be attributed to the limited number of Raman spectroscopic measurements that can be obtained from suspected mineralizing sites for a given slide when compared with mineral staining techniques. Although the amount of mineral formed at Day 14 (Figure 2b) was considered low compared with mineral formed at other time intervals (Figure 2b), it still coincided with the time point in which osteogenic Sca-1$^-$ cell cultures had previously been shown to express the osteogenic markers, ALP, and Runt-related transcription factor 2 (Runx2).[16]

The amount of mineral formed in vitro at Day 28 was comparable with that found in native calvarial tissue from PN1 mice (Figure 2b). The latter result was supported by a previous X-ray and FTIR spectroscopic study, whereby the extent of calcification formed in a 30-day-old osteoblast cell culture model, derived from embryonic chick calvaria, was similar to that found in late chick embryonic tissue and early chick postnatal tibiae.[54] In another X-ray and FTIR spectroscopic study, the mineral phase between 12-day-old MC3T3-E1 osteoblast cell cultures and 30-day-old mouse calvarial tissues were also reported to be similar.[19]

In contrast, the reason into why the mineral/matrix ratio of PN56 mice trended lower compared with PN1 mice and mineral formed in vitro at Day 28 was not initially apparent (Figure 2b). In a previous Raman spectroscopic study, calvarial tissues from PN1, PN3, PN7,

and PN14 mice exhibited similar mineral/matrix ratios (around 960/1,665 cm^{-1} ratios), but the ratios were still significantly lower when compared with 6-month-old calvarial tissue.[55] Interestingly, another study reported that trypsinized collagen extracts from 6-month-old mouse calvarial tissue were not completely mineralized, indicating that nonmineralized areas coexisted next to mineralized collagen.[56] We conjecture that the low mineral/matrix ratio exhibited by PN56 mice was the result of incomplete mineralization of parietal bone. More specifically, the cranial vault of PN56 mice may have still been expanding to accommodate the growing brain,[57] and therefore new parietal bone formed outwards from the sagittal suture region may not have been completely mineralized, leading to lower mineral/matrix ratios.

Although the current study and prior work have primarily focused on evaluating the mineralization capacity specific to Sca-1$^-$ cells under osteogenic differentiation conditions,[16,17] studies into how this in vitro osteogenic model compares with other established osteoblast cell lines or primary cell cultures have yet to be performed.[58,59] Notwithstanding, the immortalized preosteoblast MC3T3-E1 cell line has also been shown to express the stem cell marker, Sca-1, which is not unexpected given that this cell line is also derived from newborn mouse calvaria.[18] Given that both Sca-1$^-$ and MC3T3-E1 cells also express the early osteogenic differentiation markers, Runx2 and ALP,[16,17,60] suggest that these cell phenotypes would share similar mineralization outcomes in vitro. Although MC3T3-E1 cell cultures exhibit cell proliferation rates and mineralization outcomes that were comparable with those reported for primary HOb cells, ALP activity and Runx2 gene expression were, however, significantly different because of species-specific differences.[60] On the other hand, continuous cell passaging studies have shown that MC3T3-E1 cells can retain their osteogenic capacity up to 30 passages,[61] whereas Sca-1$^-$ cells lose their ability to differentiate into bone at 6 passages.[16] Further comparative studies would still be needed to ascertain whether the limited self-renewal capacity exhibited by the Sca-1$^-$ in vitro osteogenic model would better reflect the inherent heterogeneity exhibited by bone formed in vitro by primary HOb cells.[59]

3.5 | Mineral crystallinity and mineral phase

In bone Raman spectroscopy, bandwidths of the mineral $v_1(PO_4^{3-})$ peaks can convey information on mineral crystallinity, with narrower bandwidths reflecting more ordered mineral crystallites.[62] Moreover, Raman

measure of mineral crystallinity has been shown to be linearly correlated with (a) mineral crystal size measurements obtained by X-ray diffraction[63,64] and (b) percent of B-type carbonate (CO_3) content of synthetic carbonated HAs (0.3–8% CO_3).[65,66] As discussed previously, bone mineral was not detected until Day-8, and, therefore, the bandwidth measurements shown at Day 1 and Day 4 in Figure 2c (13.9 ± 3.3 and 13.8 ± 0.5 cm^{-1}, respectively) reflect those of the faint ECM matrix band and not of actual bone mineral. As shown in Figure 2c, mineral formed at Day 8 was found to be crystalline (17.8 ± 1.2 cm^{-1}), but still within the ranges found for native calvarial bone from PN1 and P56 mice (15.4 ± 0.4 and 18.6 ± 0.2 cm^{-1}, respectively), At Days 14, 17, and 25, bone mineral became less crystalline (24.0 ± 0.5, 23.7 ± 0.5, and 22.5 ± 4.0 cm^{-1}, respectively). At Day 28, bone mineral crystallinity (17.8 ± 0.5 cm^{-1}) was comparable with PN1 and PN56 mice. Narrower ranges in mineral crystallinity values reported for certain osteoblast-like cell lines have, in part, been associated with dystrophic mineral precipitations.[53] However, cell culture and postnatal mineral crystallinity measurements found in this study were considerably broader when compared with synthetic HA standard (10.1 ± 0.01 cm^{-1}).

With temporal variations in bone mineral crystallinity shown in Figure 2c, one would also expect to find variations in the corresponding mineral $v_1(PO_4^{3-})$ band positions. In our previous study involving the in vitro intramembranous mineralization of calvarial tissues from 18.5 fetal-day-old mice, we found that band positions at ~955 cm^{-1} was indicative of octacalcium phosphate (OCP)-like mineral phases, whereas band positions between 957 and 962 cm^{-1} reflected more mature, carbonated-apatitic mineral phases.[25] The temporal maturation of precursor mineral phases has been reported in other osteogenic models.[27,67] By regressing the mineral crystallinity parameter against band positions gave rise to a significant and positive linear correlation ($R^2 = 0.87$, $p < 0.001$) (Figure 2d). The plot shows that mineral phases formed in culture at Days 8 and 28 and in calvarial tissue from PN1 and PN56 mice were mature. In contrast, mineral phases formed in culture at Days 14, 17, and 25 were less mature and more OCP-like. The regression plot also included the HA standard, which was found to be highly crystalline. However, as shown in Figure S2e, the HA standard was deficient in B-type carbonate substitution unlike bone mineral formed at Day 28 (Figure 1n) and calvarial tissue from PN1 and PN56 mice (Figure S2f-g), which contained the $v_1(CO_3^{2-})$ band at ~1,070 cm^{-1}. Taken together, we show that mineral crystallinity is strongly related with the phase of the mineral formed in culture.

3.6 | Collagen crosslinks ratio

The quality of bone matrix and the degree of mineral formed in vivo are linked to the relative divalent to trivalent collagen crosslinks content.[68] Divalent collagen crosslinks are reducible intermediates, which include dehydro-dihydroxylysinonorleucine (deH-DHLNL) and dehydro-hydroxylysinonorleucine (deH-HLNL).[69] With time, these divalent collagen crosslinks mature into the more stable trivalent collagen crosslinks, which include pyridinoline (PYD) and deoxypyridinoline (DPD), amongst others.[70] The relative amounts of trivalent (PYD) to divalent (deH-DHLNL) collagen crosslinks can be estimated spectroscopically from the ratio of the deconvolved amide I bands at ~1,667 cm^{-1} and ~1,693 cm^{-1}, respectively.[71] At present, spectroscopic measures of collagen crosslinks ratios have predominantly been obtained from mineralizing and nonmineralizing MC3T3-E1 osteoblastic cell line.[72–74] As shown in Figure 2e, collagen crosslinks ratios were unremarkably consistent throughout the 28-day culture period, with the exception of the large variation observed at Day 4. In general, collagen crosslinks ratio found at Day 28 was comparable with that found in calvarial tissue from PN1 mice but was nonsignificantly lower when compared with PN56 mice. Although age-related changes in collagen crosslink content in calvarial tissues from postnatal mice have yet to be examined, recent chromatographic analyses have shown that calvarial tissues obtained from adult mice contained higher amounts of immature collagen crosslinks compared with long bones.[75,76] In addition, older calvarial tissues have been reported to exhibit higher osteoclastic activity compared with long bones, which could in part explain why collagen crosslinks ratios found in PN56 mice were considerably lower when compared with PN1 mice.

3.7 | Collagen disorder/order ratio

The spectral region between 1,200 and 1,300 cm^{-1} was also found to contain information on the conformation of proteins expressed by Sca-1$^-$ cells, either internally or externally. As shown in Figure 2f, the ratio between the amide III subbands at ~1,246 cm^{-1} (β-sheet, disordered structure) and ~1,264 cm^{-1} (α-helix, ordered structure)[32,34] were used to evaluate (a) the relative amounts of disordered to ordered proteins expressed by Sca-1$^-$ cells between Days 1 and 4 and (b) the structural organization of the collagenous matrix during the mineralization phase through Days 8–28. First, the high initial disorder/order ratio displayed at Day 1 was attributed to the high initial expression of disordered proteins by Sca-1$^-$ cells.

This was not entirely unexpected given that osteogenic cultures were known to be more active during the early cell proliferation phase.[52] Although changes in cell protein conformations are essential for the normal functioning of cell processes,[77,78] we speculate that the reduced disorder/order ratio found at Day 4 was attributed to the increased expression of more ordered proteins by Sca-1⁻ cells. More ordered proteins would also include α-helical collagen, which is known to be formed within days of osteogenic induction in culture.[52,79,80] The disorder/order ratios continued to decline steadily through Days 8–28, which was facilitated by the progressive stabilization and coalignment of the collagen fibrils with the apatitic mineral crystallites. Interestingly, the disorder/order ratio found in culture at Day 28 was significantly higher than those of calvarial tissue from PN1 and PN56 mice. These differences could in part be explained by the fact that bone mineral formed in two-dimensional osteogenic cell cultures do not fully capture the hierarchical or anisotropic collagen organization found in native bone.[81–83] A recent in situ second-harmonic-generation study has also shown that collagen fibers produced by preosteoblast MC3T3-E1 cell cultures are in general less structured and nonspecifically orientated due to immature structure.[84] In addition, the collagen amide III band at ~1,270 cm⁻¹ is known to be strongly polarization-dependent compared with the ~1,240 cm⁻¹ band[36,37] and therefore would be more sensitive to the orientation of collagen fibrils, especially in native bone. It has recently been shown that the orientation and alignment of cells in osteogenic culture can be increased by using artificially orientated collagen scaffolds[85] or by mechanical stimulation.[86] These tissue-engineering approaches could be employed to provide tissues with the higher degree of anisotropic collagen found in native bone.

3.8 | Limitation of the current study

Although mineral crystallinity of bone formed by Sca-1⁻ cell cultures and postnatal bone were found to be linearly correlated with mineral band position (Figure 2d), the high initial mineral/matrix ratios observed at Day 8 (Figure 2b) still requires further investigation. More specifically, the current study would have benefited from additional replicate experiments to determine whether the high initial mineral/matrix ratios observed at Day 8 was an outlier or related to the normal biological variation inherent to Sca-1⁻ stem/progenitor cells isolated fetal mouse calvarial tissues. Previous in vivo organ culture spectroscopic studies have also shown that the mineralization and mineral crystallinity kinetics of neonatal mouse calvarias are different. In the latter study,

mineral/matrix ratios was found to increase in aperiodic step-like increments over a 6-day period, whereas mineral crystallinity increased linearly before reaching a plateau around Day 3.[23]

4 | CONCLUSIONS

The current work shows that osteogenic cell cultures, enriched by calvarial-derived Sca-1⁻ stem/progenitor cells, can produce bone that is comparable with 1-day-old postnatal bone in terms of mineralization, mineral crystallinity, and collagen crosslink ratios. Additional new insights into the mineral phase of the cell cultures could be obtained by regressing the mineral crystallinity parameter against the mineral band position. Raman spectra of osteogenic cell cultures were found to be considerably more complex with the detection of additional triglyceride and glycosaminoglycan-like components. Through the characterization of cell- and collagen-specific vibrational modes, we show that the downregulation of cell activity preceded mineralization. However, osteogenic cell cultures could not fully replicate the high degree of collagen fibril order found in native bone. Further investigation into using orientated collagen scaffolds or mechanical stimulation maybe required to produce bone with increased collagen fibril order that is inherent to native bone. In conclusion, our data provides new insights into the composition of osteogenic cell cultures and the quality of mineral and matrix formed by Sca-1⁻ stem/progenitor cells. Raman spectroscopic measures of bone quality used in this study could equally be used to evaluate ex vivo specimens obtained from preclinical models that are used in tissue engineering research.

CONFLICT OF INTEREST

AUTHOR CONTRIBUTIONS

Study concept, design, and provision of study materials: M. D.M. and M.A.I. Sca-1$^-$ cell culture model development: M.A.I. and P.S. Cell isolation and culturing: P.S. Histochemistry: P.S, G.S.M. Raman data collection and analysis: G.S.M. Data interpretation: G.S.M., P.S., M.D.M., and M.A. I. Manuscript writing: G.S.M., P.S., and M.D.M.

ORCID

Gurjit S. Mandair https://orcid.org/0000-0001-8765-6624

REFERENCES

[1] V. Allareddy, R. P. Nalliah, *J. Oral Maxillofac. Surg.* **2011**, *69*, 2613.

[2] A. O. M. Wilkie, G. M. Morriss-Kay, *Nat. Rev. Genet.* **2001**, *2*, 458.

[3] E. I. Lee, A. H. Chao, R. J. Skoracki, P. R. Yu, F. DeMonte, M. M. Hanasono, *Plast. Reconstr. Surg.* **2014**, *133*, 675.

[4] S. N. Khan, F. P. Cammisa, H. S. Sandha, A. D. Diwan, F. P. Girardi, J. M. Lane, *J. Am. Acad. Orthop. Surg.* **2005**, *13*, 77.

[5] M. A. Riordan, V. M. Simpson, W. A. Hall, *World Neurosurg.* **2016**, *87*, 207.

[6] D. J. Bonda, S. Manjila, W. R. Selman, D. Dean, *Neurosurgery* **2015**, *77*, 814.

[7] B. A. Fishero, N. Kohli, A. Das, J. J. Christophel, Q. J. Cui, *Craniomaxillofac Trauma Reconstr.* **2015**, *8*, 23.

[8] E. S. Place, N. D. Evans, M. M. Stevens, *Nat. Mater.* **2009**, *8*, 457.

[9] L. Santos-Ruiz, D. J. Mowatt, A. Marguerie, D. Tukiainen, M. Kellomaki, P. Tormala, E. Suokas, H. Arstila, N. Ashanunakhi, P. Ferretti, *J. Tissue Eng. Regen. Med.* **2007**, *1*, 199.

[10] D. Marolt, M. Knezevic, G. V. Novakovic, *Stem Cell Res. Ther.* **2010**, 1.

[11] B. Levi, J. P. Glotzbach, V. W. Wong, E. R. Nelson, J. Hyun, D. C. Wan, G. C. Gurtner, M. T. Longaker, *J. Craniofac. Surg.* **2012**, *23*, 319.

[12] F. Anjos-Afonso, D. Bonnet, *Best Pract. Res., Clin. Haematol.* **2011**, *24*, 13.

[13] J. A. Helms, R. R. Amasha, P. Leucht, *Bone* **2007**, *41*, 479.

[14] F. M. Chen, L. A. Wu, M. Zhang, R. Zhang, H. H. Sun, *Biomaterials* **2011**, *32*, 3189.

[15] C. Holmes, W. L. Stanford, *Stem Cells* **2007**, *25*, 1339.

[16] P. Steenhuis, G. J. Pettway, M. A. Ignelzi, *Calcif. Tissue Int.* **2008**, *82*, 44.

[17] P. Steenhuis, K. M. Carr, G. J. Pettway, M. A. Ignelzi, *Cells Tissues Organs* **2009**, *190*, 150.

[18] M. C. Horowitz, A. Fields, D. Demeo, H. Y. Qian, A. L. M. Bothwell, E. Trepman, *Endocrinology* **1994**, *135*, 1032.

[19] W. N. Addison, V. Nelea, F. Chicatun, Y. C. Chien, N. Tran-Khanh, M. D. Buschmann, S. N. Nazhat, M. T. Kaartinen, H. Vali, M. M. Tecklenburg, R. T. Franceschi, M. D. McKee, *Bone* **2015**, *71*, 244.

[20] L. F. Bonewald, S. E. Harris, J. Rosser, M. R. Dallas, S. L. Dallas, N. P. Camacho, B. Boyan, A. Boskey, *Calcif. Tissue Int.* **2003**, *72*, 537.

[21] C. C. Moura, R. S. Tare, R. O. C. Oreffo, S. Mahajan, *J. R. Soc, Interface* **2016**, *13*.

[22] A. Hashimoto, L. D. Chiu, K. Sawada, T. Ikeuchi, K. Fujita, M. Takedachi, Y. Yamaguchi, S. Kawata, S. Murakami, E. Tamiya, *J. Raman Spectrosc.* **2014**, *45*, 157.

[23] J. D. P. McElderry, G. S. Zhao, A. Khmaladze, C. G. Wilson, R. T. Franceschi, M. D. Morris, *J. Bone Miner. Res.* **2013**, *28*, 1846.

[24] P. S. Hung, Y. C. Kuo, H. G. Chen, H. H. K. Chiang, O. K. S. Lee, *PLoS One* **2013**, *8*.

[25] N. J. Crane, V. Popescu, M. D. Morris, P. Steenhuis, M. A. Ignelzi Jr., *Bone* **2006**, *39*, 434.

[26] F. Draux, P. Jeannesson, A. Beljebbar, A. Tfayli, N. Fourre, M. Manfait, J. Sule-Suso, G. D. Sockalingum, *Analyst* **2009**, *134*, 542.

[27] S. J. Smith, R. Emery, A. Pitsillides, C. E. Clarkin, S. Mahajan, *Analyst* **2017**, *142*, 1962.

[28] L. Lammers, C. Naujoks, K. Berr, R. Depprich, N. Kubler, U. Meyer, F. Langenbach, B. Luttenberg, G. Kogler, H. P. Wiesmann, J. Handschel, *Stem Cell Res.* **2012**, *8*, 193.

[29] C. A. Luppen, E. Smith, L. Spevak, A. L. Boskey, B. Frenkel, *J. Bone Miner. Res.* **2003**, *18*, 1186.

[30] L. L. McManus, G. A. Burke, M. M. McCafferty, P. O'Hare, M. Modreanu, A. R. Boyd, B. J. Meenan, *Analyst* **2011**, *136*, 2471.

[31] G. S. Mandair, M. D. Morris, *BoneKEy Rep.* **2015**, *4*.

[32] Z. Movasaghi, S. Rehman, I. U. Rehman, *Appl. Spectrosc. Rev.* **2007**, *42*, 493.

[33] S. Gamsjaeger, K. Klaushofer, E. P. Paschalis, *J. Raman Spectrosc.* **2014**, *45*, 794.

[34] G. S. Mandair, A. L. Han, E. T. Keller, M. D. Morris, *J. Biomed. Opt.* **2016**, *21*, 115001.

[35] C. Y. Wang, Y. Wang, N. T. Huffman, C. Y. Cui, X. M. Yao, S. Midura, R. J. Midura, J. P. Gorski, *J. Biol. Chem.* **2009**, *284*, 7100.

[36] A. Bonifacio, V. Sergo, *Vib. Spectrosc.* **2010**, *53*, 314.

[37] T. Colard, G. Falgayrac, B. Bertrand, S. Naji, O. Devos, C. Balsack, Y. Delannoy, G. Penel, *PLoS One* **2016**, *11*, e0167316.

[38] D. R. Rux, J. Y. Song, K. M. Pineault, G. S. Mandair, I. T. Swinehart, A. J. Schlientz, K. N. Garthus, S. A. Goldstein, K. M. Kozloff, D. M. Wellik, *J. Bone Miner. Res.* **2017**, *32*, 1750.

[39] N. Fratzl-Zelman, P. Fratzl, H. Horandner, B. Grabner, F. Varga, A. Ellinger, K. Klaushofer, *Bone* **1998**, *23*, 511.

[40] K. Satomura, M. Nagayama, *Acta Anat.* **1991**, *142*, 97.

[41] M. E. Marsh, A. M. Munne, J. J. Vogel, Y. Q. Cui, R. T. Franceschi, *J. Bone Miner. Res.* **1995**, *10*, 1635.

[42] C. Krafft, L. Neudert, T. Simat, R. Salzer, *Spectrochim. Acta, Part A* **2005**, *61*, 1529.

[43] A. During, G. Penel, P. Hardouin, *Prog. Lipid Res.* **2015**, *59*, 126.

[44] K. H. Mroue, J. D. Xu, P. Z. Zhu, M. D. Morris, A. Ramamoorthy, *Phys. Chem. Chem. Phys.* **2016**, *18*, 18687.

[45] D. M. Wen, C. Androjna, A. Vasanji, J. Belovich, R. Midura, *Ann. Biomed. Eng.* **2010**, *38*, 558.

[46] Y. Tintut, L. L. Demer, *Trends Endocrinol. Metab.* **2014**, *25*, 53.

[47] H. Nakamura, A. Hirata, T. Tsuji, T. Yamamoto, *Arch. Histol. Cytol.* **2001**, *64*, 109.

[48] P. Blumberg, R. Brenner, S. Budny, H. Kresse, *Calcif. Tissue Int.* **1997**, *60*, 554.

[49] K. J. Manton, L. M. Haupt, K. Vengadasalam, V. Nurcombe, S. M. Cool, *J. Mol. Histol.* **2007**, *38*, 415.

[50] H. D. Nah, M. Pacifici, L. C. Gerstenfeld, S. L. Adams, T. Kirsch, *J. Bone Miner. Res.* **2000**, *15*, 522.

[51] H. G. Schulze, S. O. Konorov, N. J. Caron, J. M. Piret, M. W. Blades, R. F. B. Turner, *Anal. Chem.* **2010**, *82*, 5020.

[52] G. S. Stein, J. B. Lian, T. A. Owen, *FASEB J.* **1990**, *4*, 3111.

[53] L. L. McManus, F. Bonnier, G. A. Burke, B. J. Meenan, A. R. Boyd, H. J. Byrne, *Analyst* **2012**, *137*, 1559.

[54] C. Rey, H. M. Kim, L. Gerstenfeld, M. J. Glimcher, *Connect. Tissue Res.* **1996**, *35*, 343.

[55] C. P. Tarnowski, M. A. Ignelzi, M. D. Morris, *J. Bone Miner. Res.* **2002**, *17*, 1118.

[56] B. Zimmermann, A. Moegelin, P. de Souza, J. Bier, *Anat. Embryol.* **1998**, *197*, 155.

[57] K. A. Lenton, R. P. Nacamuli, D. C. Wan, J. A. Helms, M. T. Longaker, *Curr. Top Dev. Biol* **2005**, *66*, 287.

[58] S. Zhu, S. Ehnert, M. Rouß, V. Häussling, R. Aspera-Werz, T. Chen, A. Nussler, *Int. J. Mol. Sci.* **2018**, *19*, 2284.

[59] E. M. Czekanska, M. J. Stoddart, R. G. Richards, J. S. Hayes, *Eur. Cells Mater* **2012**, *24*, 1.

[60] E. M. Czekanska, M. J. Stoddart, J. R. Ralphs, R. G. Richards, J. S. Hayes, J. Biomed, *Mater. Res., Part A* **2014**, *102*, 2636.

[61] X. Z. Yan, W. X. Yang, F. Yang, M. Kersten-Niessen, J. A. Jansen, S. K. Both, *Tissue Eng., Part C* **2014**, *20*, 198.

[62] J. J. Freeman, B. Wopenka, M. J. Silva, J. D. Pasteris, *Calcif. Tissue Int.* **2001**, *68*, 156.

[63] Y. Sa, Y. R. Guo, X. W. Feng, M. Wang, P. Li, Y. X. Gao, X. Yang, T. Jiang, *New J. Chem.* **2017**, *41*, 5723.

[64] H. Aguiar, S. Chiussi, M. Lopez-Alvarez, P. Gonzalez, J. Serra, *Ceram. Int.* **2018**, *44*, 495.

[65] M. M. Wang, R. Qian, M. Bao, C. X. Gu, P. Z. Zhu, *Mater. Lett.* **2018**, *210*, 203.

[66] A. Awonusi, M. D. Morris, M. M. J. Tecklenburg, *Calcif. Tissue Int.* **2007**, *81*, 46.

[67] M. Bennet, A. Akiva, D. Faivre, G. Malkinson, K. Yaniv, S. Abdelilah-Seyfried, P. Fratzl, A. Masic, *Biophys. J.* **2014**, *106*, L17.

[68] M. Saito, K. Marumo, *Osteoporosis Int.* **2010**, *21*, 195.

[69] T. J. Sims, N. C. Avery, A. J. Bailey, in *Extracellular Matrix Protocols*, (Eds: C. H. Streuli, M. E. Grant), Humana Press, Totowa, New Jersey **2000** 11.

[70] E. P. Paschalis, S. Gamsjaeger, D. N. Tatakis, N. Hassler, S. P. Robins, K. Klaushofer, *Calcif. Tissue Int.* **2015**, *96*, 18.

[71] E. P. Paschalis, K. Verdelis, S. B. Doty, A. L. Boskey, R. Mendelsohn, M. Yamauchi, *J. Bone Miner. Res.* **2001**, *16*, 1821.

[72] Y. Z. Meng, M. E. Faillace, K. Dorst, S. J. Palmaccio, L. M. Miller, Y. X. Qin, *Biointerphases* **2017**, *12*, 031001.

[73] S. P. Canelon, J. M. Wallace, *PLoS One* **2016**, *11*, e0166392.

[74] E. M. B. McNerny, B. Gong, M. D. Morris, D. H. Kohn, *J. Bone Miner. Res.* **2015**, *30*, 446.

[75] T. van den Bos, D. Speijer, R. A. Bank, D. Bromme, V. Everts, *Bone* **2008**, *43*, 459.

[76] T. Matsuura, K. Tokutomi, M. Sasaki, M. Katafuchi, E. Mizumachi, H. Sato, *BioMed Res. Int* **2014**.

[77] F.-X. Theillet, A. Binolfi, T. Frembgen-Kesner, K. Hingorani, M. Sarkar, C. Kyne, C. Li, P. B. Crowley, L. Gierasch, G. J. Pielak, A. H. Elcock, A. Gershenson, P. Selenko, *Chem. Rev.* **2014**, *114*, 6661.

[78] S. R. Panikkanvalappil, S. M. Hira, M. A. Mahmoud, M. A. El-Sayed, *J. Am. Chem. Soc.* **2014**, *136*, 15961.

[79] R. T. Franceschi, B. S. Iyer, *J. Bone Miner. Res.* **1992**, *7*, 235.

[80] L. D. Quarles, D. A. Yohay, L. W. Lever, R. Caton, R. J. Wenstrup, *J. Bone Miner. Res.* **1992**, *7*, 683.

[81] B. G. Matthews, D. Naot, K. E. Callon, D. S. Musson, R. Locklin, P. A. Hulley, A. Grey, J. Cornish, *BoneKEy Rep.* **2014**, *3*, 560.

[82] D. Zujur, K. Kanke, A. C. Lichtler, H. Hojo, U. Chung, S. Ohba, *Sci. Adv.* **2017**, *3*.

[83] E. Gentleman, R. J. Swain, N. D. Evans, S. Boonrungsiman, G. Jell, M. D. Ball, T. A. V. Shean, M. L. Oyen, A. Porter, M. M. Stevens, *Nat. Mater.* **2009**, *8*, 763.

[84] E. Hase, O. Matsubara, T. Minamikawa, K. Sato, T. Yasui, *Appl. Opt.* **2016**, *55*, 3261.

[85] R. Ozasa, A. Matsugaki, Y. Isobe, T. Saku, H.-S. Yun, T. Nakano, J. Biomed, *Mater. Res., Part A.* **2018**, *106*, 360.

[86] Y. Uto, S. Kuroshima, T. Nakano, T. Ishimoto, N. Inaba, Y. Uchida, T. Sawase, *PLoS One* **2017**, *12*, e0189893.

SUPPORTING INFORMATION

Additional supporting information may be found online in the Supporting Information section at the end of the article.

How to cite this article: Mandair GS, Steenhuis P, Ignelzi Jr MA, Morris MD. Bone quality assessment of osteogenic cell cultures by Raman microscopy. *J Raman Spectrosc.* 2019;50:360–370. https://doi.org/10.1002/jrs.5521